THE JOURNAL OF PHYSICAL CHEMISTRY B

Article

pubs.acs.org/JPCB

Aggregation Behavior of Triton X-100 with a Mixture of Two Room-Temperature Ionic Liquids: Can We Identify the Mutual Penetration of Ionic Liquids in Ionic Liquid Containing Micellar Aggregates?

Vishal Govind Rao, Sarthak Mandal, Surajit Ghosh, Chiranjib Banerjee, and Nilmoni Sarkar*

Department of Chemistry, Indian Institute of Technology, Kharagpur 721302, WB, India

Supporting Information

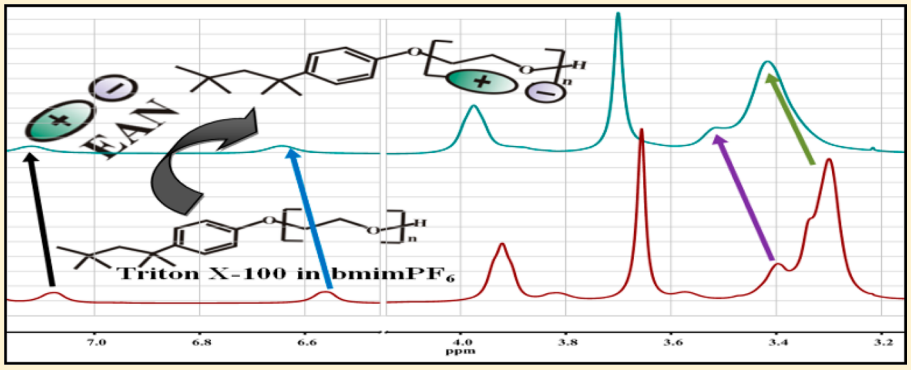

ABSTRACT: In this manuscript, we have characterized two different micellar aggregates containing all nonvolatile components. We have shown (i) the effect of ethylammonium nitrate (EAN) addition on the properties of micellar solution of Triton X-100 in 1-butyl-3-methylimidazolium hexafluorophosphate ($bmimPF_6$) and (ii) the effect of $bmimPF_6$ addition on the properties of micellar solution of Triton X-100 in EAN. To investigate the effect, we have used ^1H NMR, pulsed-field gradient spin−echo NMR (PFGSE NMR), and methyl orange (MO) and coumarin 153 (C-153) as absorption and emission probes, respectively. The penetration of added EAN inside the Triton X-100/$bmimPF_6$ micellar aggregates is indicated by (i) red shift in both the absorption spectra of MO and emission spectra of C-153 and (ii) downfield shift of proton signals of ethylene oxide units in Triton X-100. On the other hand, ^1H NMR and PFGSE NMR indicates the penetration of added $bmimPF_6$ inside the Triton X-100/EAN micellar aggregates. However, the constancy of both the absorption spectra of MO and emission spectra of C-153 indicates that the microenvironment around the probe molecules remains unaffected. We have also investigated the effect of micelle formation and the effect of penetration of ionic liquids (ILs) in micellar aggregates, on the solvation dynamics of C-153. The solvent relaxation around C-153 gets retarded on going from neat ILs to the micellar solution of Triton X-100 in ILs. In addition to this, we have also observed that with the addition of EAN in Triton X-100/$bmimPF_6$ micellar aggregates the solvation dynamics becomes faster, whereas with the addition of $bmimPF_6$ in Triton X-100/EAN micellar aggregates we did not observe any notable change in solvation dynamics. This observation further supports the conclusions drawn from UV−visible and NMR studies.

1. INTRODUCTION

The self-assembly of surfactant molecules into a large variety of nano-, micro-, and macrostructures is of central interest and plays a substantial role in many important applications such as nanomaterial synthesis,[1] drug delivery,[2] separations,[3] pharmaceutical formulations, and other dispersant technologies.[3,4] To date, there has been a limited number of solvents which are generally recognized as self-assembly media.[5,6] The majority of aggregation studies use water or volatile organic solvents as the solvent. One can increase the number of these solvents by understanding and manipulating the molecular interactions involved in amphiphile self-assembly. In fact, supercritical CO_2 (where the gas is compressed until it is nearly as dense as a liquid)[7−9] and ionic liquids (ILs) have already been utilized as alternatives to the traditional solvents.

Ionic liquids (ILs) are organic salts which have low melting points (by convention below 100 °C) due to the presence of sterically mismatched ions[10−12] that hinder crystal formation. They are often associated with "green chemistry" because they possess certain advantageous properties typically linked to environment friendly solvents like negligible vapor pressure, wide electrochemical window, nonflammability, high thermal stability, and wide liquid range.[13] They are often designated as "designer solvents" because their physical properties can be customized by incorporation of appropriate functional groups.[14,15] Research in IL containing microheterogeneous

Received: September 13, 2012
Revised: November 2, 2012
Published: November 5, 2012

systems was prompted by the fact that, despite the useful properties of ILs, poor solubility of apolar solutes in neat ILs was a major hindrance in the path of their potential application. This could be overcome using hydrocarbon domains provided by amphiphilic molecules in ionic liquids. The expected thermal stability of such a system over microheterogeneous systems containing conventional solvents was another appealing factor. Luckily, there are a number of examples appearing in the literature where ionic liquids have been used for structuring the amphiphilic molecules, namely, as micelles,[16−26] microemulsions,[27−42] vesicles,[43] and gels.[44] These aggregates certainly overcome the solubility limitations of ILs and at the same time provide hydrophobic or hydrophilic nanodomains, thereby expanding potential uses of ILs in microheterogeneous systems as reaction and extraction media.

The formation of a micelle in a RTIL, ethylammonium nitrate (EAN), by common surfactant was first documented in 1982 by Evans et al.,[16,17] whereas the formation of liquid crystals of lipids in EAN[45] as well as lyotropic liquid crystals of nonionic surfactants were observed in the same RTIL.[46] The self-aggregation of common ionic and nonionic surfactants in imidazolium-based RTIL has also been reported by different groups.[18,19,43,47−49] Gao et al. reported the micellar aggregation of Triton X-100 in 1-butyl-3-methylimidazolium hexafluorophosphate ($bmimPF_6$) and 1-butyl-3-methylimidazolium tetrafluoroborate ($bmimBF_4$).[39,50] The aggregation of the amphiphilic ionic liquids (AmIL's) in ionic liquids (ILs) is also reported. Recently, Kunz and Thomaier[22] reported the aggregation of 1-methyl-3-hexadecylimidazolium chloride ($C_{16}MIMCl$) and 1-methyl-3-hexadecylimidazolium tetrafluoroborate ($C_{16}MIMBF_4$) in their role as a surfactant and EAN as the continuous solvent. Zhao et al.[51] showed the aggregation behavior of $C_{16}MIMCl$ in EAN with increasing concentration of $C_{16}MIMCl$ and compared the phase behavior of $C_{16}MIMCl$/EAN with that of the $C_{16}MIMCl$/water binary system. Preliminary results indicated that these aggregate systems are stable at temperatures greater than 200 °C and can probably be used to extend the limited temperature range water based colloids.

In addition to the characterization of different RTIL containing microheterogeneous systems, several photophysical, theoretical, and ultrafast spectroscopic studies were carried out in RTILs and RTIL containing microheterogeneous systems.[52−58] After the first report of Samanta and co-workers,[59,60] several studies are appearing in the literature on solvation dynamics in neat RTILs.[61−63] The investigation of solvation dynamics can provide useful information regarding microheterogeneous systems. Over the last three decades, substantial efforts have been made to understand solvation dynamics in different heterogeneous media such as micelles, reverse micelles, microemulsions, lipids, proteins, DNA, etc.[64−72] Nowadays, solvation dynamics study of a newly created ion or a dipole in polar liquids is often employed for obtaining molecular level information about the response of solvent molecules (which is comprised of both orientational and translational motions) to the probe.[64−66,73] Particularly, the solvation dynamics in RTILs are immensely different from that in the isopolar conventional solvents such as methanol, acetonitrile, and water.[52,56,74,75] The dynamics in RTILs show biphasic nature having a slow nanosecond time scale component along with a subpicosecond component.[53,63,76] For the detailed understanding of the solvation process in RTILs, several groups carried out computer simulations on the structure and dynamics of a probe in a RTIL.[77−81] These studies clearly suggest that solvation dynamics in RTIL involves collective motion of cations and anions. Adhikari et al.[38] investigated the solvation dynamics in neat 1-pentyl-3-methylimidazolium tetrafluoroborate ($pmimBF_4$) and different regions of the $pmimBF_4$ containing microemulsions. Petrich and co-workers studied solvation dynamics of C-153 in surface active ionic liquids (SAILs), 1-cetyl-3-vinyl-imidazolium bromide and 1-cetyl-3-vinyl-imidazolium bis(trifluoromethylsulfonyl)imide, and their micelles in water.[82]

Inspired from the above-mentioned high temperature stable microheterogeneous systems, we have characterized micellar aggregates containing all nonvolatile components. In this manuscript, we have shown the aggregation behavior of Triton X-100 in a mixture of ILs, EAN and $bmimPF_6$. For characterization purposes, we used ^1H NMR, pulsed-field gradient spin−echo NMR (PFGSE NMR), and methyl orange (MO) as an absorption probe. In addition to this, we have also investigated the solvent relaxation dynamics in these aggregates using C-153 as a probe molecule. These systems contain all nonvolatile components, which add to the potential applicability of these green systems for carrying out chemical reactions at high temperature. Furthermore, the characterized systems can also be used for the synthesis of organic and inorganic materials at high temperature. These systems are especially attractive for reactants that may react with water undesirably.[83]

2. EXPERIMENTAL SECTION

Coumarin 153 (C-153) (laser grade, Exciton) and methyl orange (MO, Merck) were used as received. Triton X-100 (Aldrich) and $bmimPF_6$ (Kanto chemicals, 98% purity) were dried in a vacuum for 12 h at 70−80 °C before use. The RTIL, EAN, was prepared by the reaction of equimolar amounts of ethylamine and nitric acid as described by Evans et al.[16] Water was removed by rotary evaporation followed by lyophilization.

Following Gao et al.,[50] we have used 0.82 M Triton X-100 in $bmimPF_6$ to observe the effect of EAN addition (volumetric concentration of Triton X-100 changes with the addition of EAN). Gao et al.[50] showed the variation of surface tension and hence micellar aggregate formation by Triton X-100 in 1-butyl-3-methylimidazolium hexafluorophosphate ($bmimPF_6$) at 298 K. In their study, they concluded that the low solvophobicity between the ionic liquid and the hydrophobic tail of Triton X-100 is responsible for a high critical micelle concentration (CMC). The CMC of Triton X-100 in $bmimPF_6$ was found to be 0.78 M,[50] which is much higher than in water under the same condition (3.19×10^{-4} M).[84] Following Evans et al.,[16] we used 0.37 M Triton X-100 in EAN to observe the effect of $bmimPF_6$ addition (the volumetric concentration of Triton X-100 changes with the addition of $bmimPF_6$). Evans et al. reported the aggregation behavior of Triton X-100 in EAN is similar to the behavior of Triton X-100 in water.[16] They reported that the observed values of CMCs in EAN are approximately 5−10 times greater than those observed in water. They reported the CMC value of Triton X-100 at two different temperatures as 6.11 and 5.93 mM at 50 and 21 °C, respectively.

The absorption and fluorescence spectra were collected using a Shimadzu (model no. UV-2450) spectrophotometer and a Hitachi (model no. F-7000) spectrofluorimeter, respectively. The final concentration of probe molecule, C-153, in all the measurements was kept at ~3.8×10^{-6} M. ^1H NMR

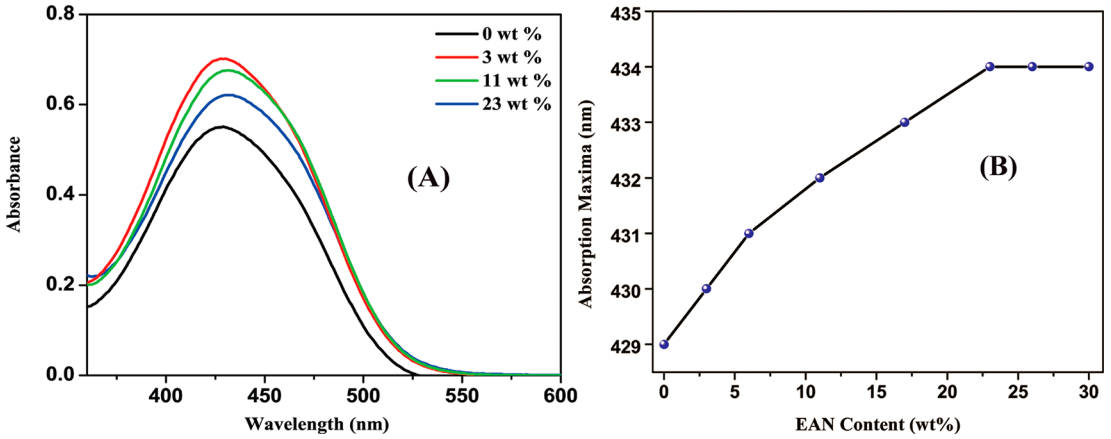

Figure 1. (A) Absorption spectra of methyl orange (MO) in the Triton X-100/bmimPF$_6$ micellar aggregates containing different amounts of EAN. (B) Variation of λ_{max} of MO in the Triton X-100/bmimPF$_6$ micellar aggregates as a function of EAN content (wt %).

measurements were carried out with a Bruker 400 MHz NMR spectrometer. In all the NMR measurements, we used D_2O as an external chemical shift reference. To remove any perturbation to the studied system arising from the presence of D_2O, D_2O was packed in a capillary and then added to the NMR tube. All the experiments were performed at 298 K.

For steady-state experiments, all the samples were excited at 408 nm. The detailed time-resolved fluorescence setup is described in our earlier publication.[85] Briefly, the samples were excited at 408 nm using a picosecond laser diode (IBH, Nanoled), and the signals were collected at the magic angle (54.7°) using a Hamamatsu microchannel plate photomultiplier tube (3809U). The instrument response function of our setup is ~90 ps. The analysis of the fluorescence decay data was performed using IBH DAS, version 6, decay analysis software. For viscosity measurements, we used a Brookfield DV-II+ Pro (viscometer). The temperature was maintained by circulating water through the cell holder using a JEIO TECH Thermostat (RW-0525GS).

3. RESULTS AND DISCUSSION

3.1. Absorption Spectra of Methyl Orange. Methyl orange (MO) is often used as a solvatochromic probe.[86] It is sensitive to the local environment, and its UV−vis absorbance maximum (λ_{max}) gets red-shifted with increasing polarity of the microenvironment. Thus, the effect of gradual addition of EAN on the microenvironment in Triton X-100/bmimPF$_6$ micellar aggregate can be demonstrated by absorption spectra of MO (Figure 1A). The absorption maximum (λ_{max}) of MO is red-shifted from 429 to 434 nm with increasing EAN content from 0 to 23 wt % (Figure 1B). With further increase of EAN content, the λ_{max} remains constant (434 nm). This can be accounted for by considering the fact that MO is not soluble in bmimPF$_6$ and, in Triton X-100/bmimPF$_6$ micellar aggregate, MO binds with the EO group of Triton X-100.[87] Thus, it is clear that the EAN molecule penetrates to Triton X-100/bmimPF$_6$ micellar aggregate and bound to the EO units, while after the bound EAN molecule reaches the saturation point, the added EAN molecules go to bulk bmimPF$_6$.

In the case of Triton X-100/EAN micellar aggregate, we noted that (i) MO is soluble in EAN, (ii) the λ_{max} of MO in neat EAN is 440 nm, and (iii) the λ_{max} in Triton X-100/EAN system is 434 nm, which indicates that the probe resides at the surface of the micellar aggregate. With gradual addition of

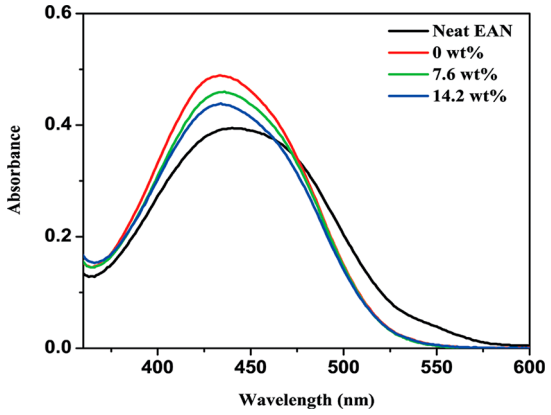

Figure 2. Absorption spectra of methyl orange (MO) in neat EAN and in the Triton X-100/EAN micellar aggregates containing different amounts of bmimPF$_6$.

bmimPF$_6$ to Triton X-100/EAN micellar aggregate, the λ_{max} remains unchanged (Figure 2). Thus, following this observation, we can propose two possibilities: (i) bmimPF$_6$ does not penetrate in Triton X-100/EAN micellar aggregates and (ii) the penetration of bmimPF$_6$ in Triton X-100/EAN micellar aggregates does not affect the local environment of MO.

3.2. ^{1}H NMR Spectra. ^{1}H NMR spectra were taken to provide more detailed information about the intermolecular interactions and thus provide the locations of the added EAN and bmimPF$_6$ molecule to Triton X-100/bmimPF$_6$ and Triton X-100/EAN micellar aggregates, respectively. Figure 3 shows ^{1}H NMR spectra of Triton X-100/bmimPF$_6$ micellar aggregate without EAN (A) and the same micellar aggregate with 11 wt % EAN (B). The chemical structure and atom numbering for bmimPF$_6$, Triton X-100, and EAN are shown in Scheme 1. When the EAN was added to the Triton X-100/bmimPF$_6$ system, the proton signal of EO units in Triton X-100 ($H_{h\text{-}y}$) shifted downfield by 0.17 ppm, whereas H_g, H_f, H_e, H_d, H_c, and H_a protons of Triton X-100 shifted by 0.14, 0.12, 0.08, 0.04, 0.03, and 0.02 ppm, respectively. The maximum change of δ value for $H_{h\text{-}y}$ protons of Triton X-100 indicates that added EAN molecules bind with the EO units of Triton X-100 and thus the electron cloud density on oxygen atoms of the EO units decreased. The carbon atoms present in the vicinity were also affected due to the induction effect. As a consequence, hydrogen atoms attached to the carbon atoms are deshielded

dx.doi.org/10.1021/jp309106a | J. Phys. Chem. B 2012, 116, 13868−13877

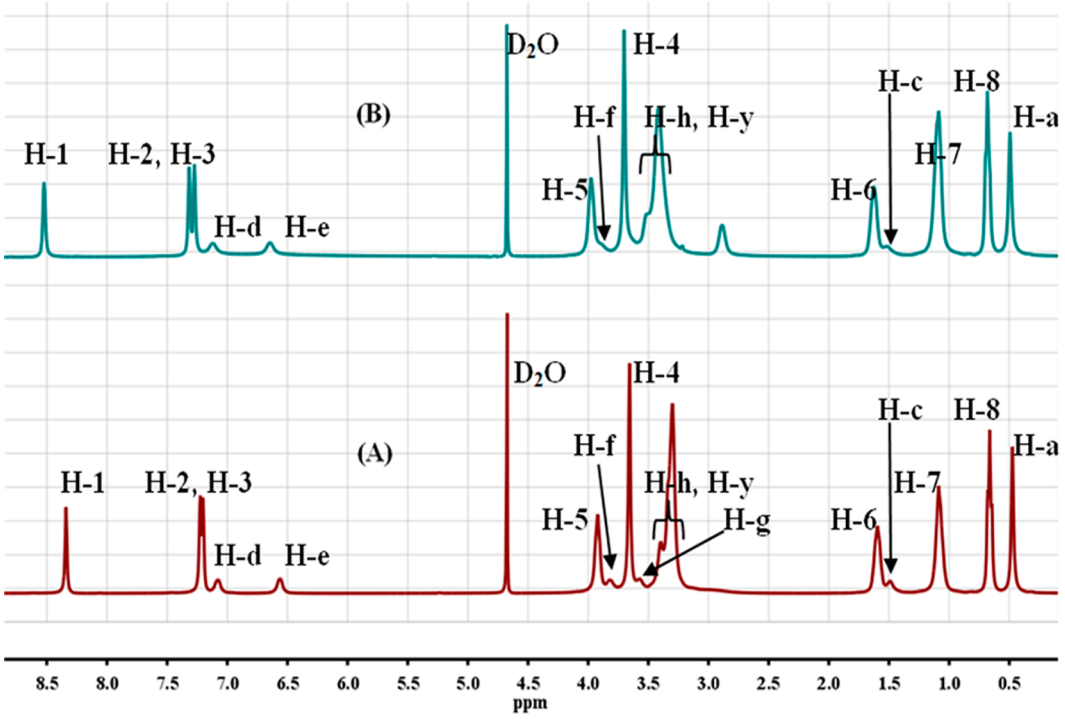

Figure 3. ^{1}H NMR spectra of Triton X-100/bmimPF$_6$ micellar aggregate without EAN (A) and the same micellar aggregate with 11 wt % EAN (B).

Scheme 1. Chemical Structure and Atom Numbering for bmimPF$_6$, Triton X-100, and EAN

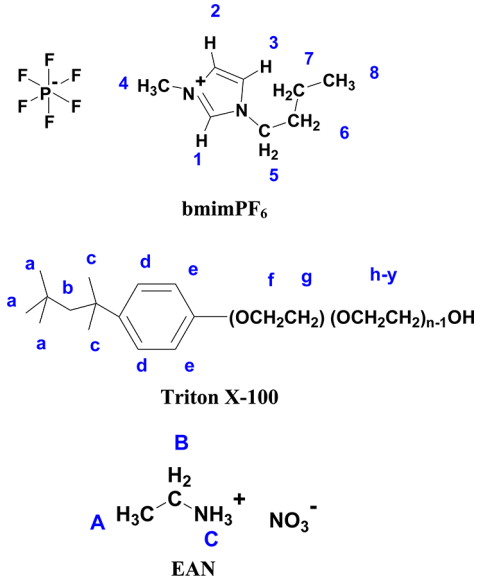

and resonate in a downfield position. Moreover, it is to be noted that the signals of all the protons of the bmim$^+$ cation were also shifted. This indicates that some of the added EAN goes into the bulk phase (bmimPF$_6$). Thus, ^{1}H NMR study also proves the penetration of Triton X-100/bmimPF$_6$ micellar aggregate by EAN. In Figure 4, we have also shown the variation of chemical shifts of $H_{h\text{-}y}$ protons of Triton X-100 against the EAN concentration. The δ value increases quite rapidly up to addition of 11 wt % EAN, whereas after the addition of 23 wt % EAN it remains almost constant. Thus, the variation of chemical shifts of $H_{h\text{-}y}$ protons of Triton X-100 indicates that the EAN molecule penetrates to the Triton X-100/bmimPF$_6$ micellar aggregate and bound to the EO units, while after the bound EAN molecule reaches the saturation point, the added EAN molecules go to bulk bmimPF$_6$. This observation corroborates with our earlier result where we have shown the variation of λ_{max} of MO in the Triton X-100/bmimPF$_6$ micellar aggregates as a function of EAN content (wt %).

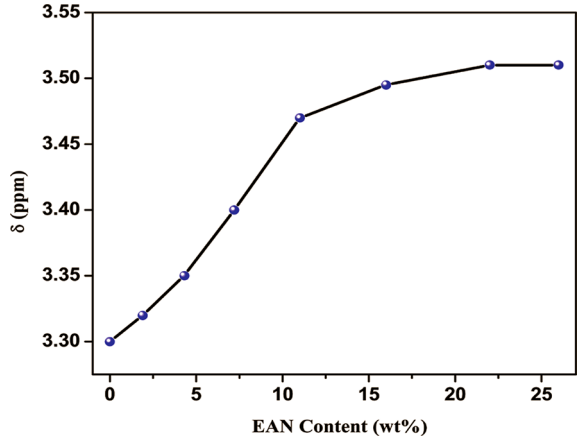

Figure 4. ^{1}H NMR chemical shifts of $H_{h\text{-}y}$ protons of Triton X-100/bmimPF$_6$ micellar aggregate as a function of EAN content (wt %).

Figure 5 shows ^{1}H NMR spectra of Triton X-100/EAN micellar aggregate without bmimPF$_6$ (A) and the same micellar aggregate with 12% bmimPF$_6$ (B). When bmimPF$_6$ was added to the Triton X-100/EAN system, all the proton signals were shifted upfield. The maximum upfield shift was observed for the H_a proton which indicates that bmimPF$_6$ goes inside the Triton X-100/EAN micellar aggregate. Here, the signals of all the protons of the ethylammonium cation were shifted (upfield) by almost the same extent as the protons of Triton X-100, which indicates that a major portion of added bmimPF$_6$ goes to the

dx.doi.org/10.1021/jp309106a | J. Phys. Chem. B 2012, 116, 13868−13877

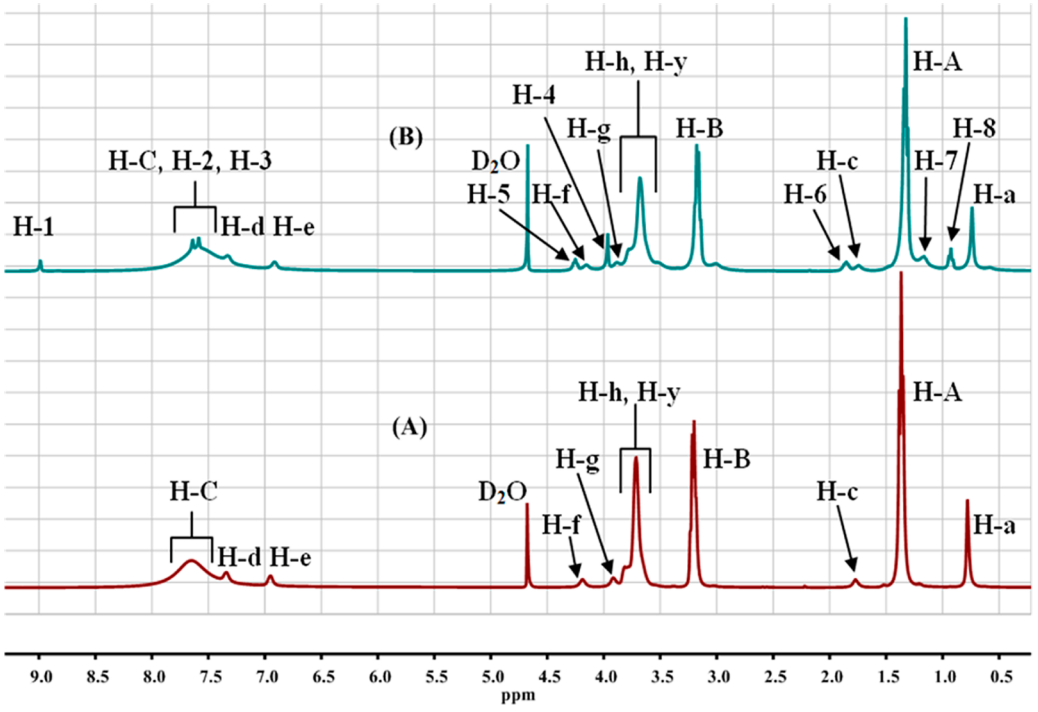

Figure 5. ^{1}H NMR spectra of Triton X-100/EAN micellar aggregate without bmimPF$_6$ (A) and the same micellar aggregate with 12 wt % bmimPF$_6$ (B).

bulk solution (EAN). This is also supported by the observed peak positions of H_1, H_2, and H_3 protons of bmimPF$_6$, which appear at 8.99, 7.64, and 7.59, respectively (Figure 5), and are very close to the value of bmimPF$_6$ in EAN (spectra not shown here).

3.3. Pulsed-Field Gradient Spin−Echo NMR (PFGSE NMR) Spectra. We used the pulsed-field gradient spin−echo NMR (PFGSE NMR) technique to determine the diffusion coefficient of bmim$^+$ cation in neat bmimPF$_6$ and bmimPF$_6$ in Triton X-100/EAN micellar aggregate, following the intensity variation of the H-1 peak in ^{1}H NMR. Due to the overlap of ^{1}H NMR signals of EAN with that of Triton X-100/bmimPF$_6$ micellar aggregate, we were not able to get the diffusion coefficient of ethylammonium cation. Self-diffusion coefficients were obtained by varying the gradient strength (g) while keeping the gradient pulse length (δ) and the gradient pulse interval constant within each experimental run. The data were fitted according to the Stejskal−Tanner equation:

$$I/I_0 = \exp\left[-Dq^2\left(\Delta - \frac{\delta}{3}\right)\right] \quad (1)$$

where I and I_0 are the signal intensities in the presence and absence of the applied field gradient, respectively, $q = \gamma g\delta$ is the so-called scattering vector, γ is the gyromagnetic ratio of the observed nucleus, $t = (\Delta - \delta/3)$ is the diffusion time, Δ is the delay between the encoding and decoding gradients, and D is the self-diffusion coefficient to be extracted.[88] In our experiments, δ and Δ were fixed at 5 and 50 ms, respectively. The variation of $\ln(I/I_0)$ versus g^2 is shown in Figure 6, and the diffusion coefficient of bmim$^+$ cation is calculated by the slope of the plot. The diffusion data for the bmim$^+$ cation is shown in Table 1. The diffusion coefficients of bmim$^+$ cation in neat bmimPF$_6$ and bmimPF$_6$ in Triton X-100/EAN micellar aggregate were found to be 3.16×10^{-11} and 1.16×10^{-11} m^2 s^{-1}, respectively.

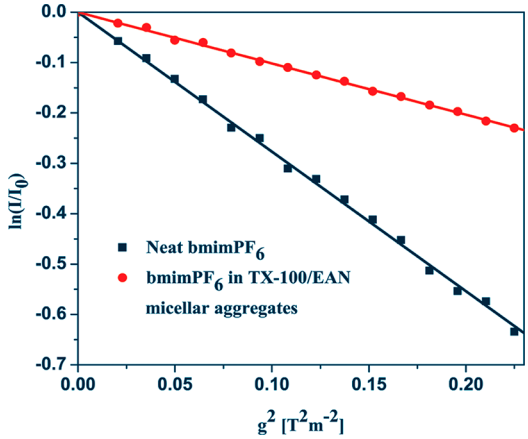

Figure 6. Variation of $\ln(I/I_0)$ versus g^2 for neat bmimPF$_6$ and bmimPF$_6$ in Triton X-100/EAN micellar aggregate.

Table 1. Diffusion Coefficient of bmim$^+$ Cation and Viscosity for Neat bmimPF$_6$ and bmimPF$_6$ in Triton X-100/EAN Micellar Aggregate at 25 °C

system	D_{bmim^+}[a] (10^{-11} m^2 s^{-1})	viscosity (cP)
neat bmimPF$_6$	3.16	155 ± 6
bmimPF$_6$ in Triton X-100/EAN micellar aggregate	1.16	81 ± 2

[a]Error in experimental data of ±10%.

The diffusion coefficient, D, can be related to the viscosity of the solution, η, by the Stokes−Einstein equation on the basis of the hydrodynamic model that a solute sphere moves through a continuum fluid

dx.doi.org/10.1021/jp309106a | J. Phys. Chem. B 2012, 116, 13868−13877

$$D = \frac{k_B T}{6\pi r \eta} \quad (2)$$

The viscosity values of neat bmimPF$_6$ and bmimPF$_6$ in Triton X-100/EAN micellar aggregate were found to be 155 and 81 cP, respectively. In our case, the viscosity decreases, almost by a factor of 2, on going from neat bmimPF$_6$ to bmimPF$_6$ in the Triton X-100/EAN micellar aggregate. Thus, if there is no other factor which reduces the diffusion coefficient of bmim$^+$ cation, then we should get 2-fold increments in the diffusion coefficient of bmim$^+$ cation (if we consider the Triton X-100/EAN micellar aggregate as a sphere). On the contrary, we found that the diffusion coefficient of bmim$^+$ cation reduces, almost by a factor of 3. This clearly indicates that bmimPF$_6$ penetrates Triton X-100/EAN micellar aggregate.

3.4. Absorption and Steady-State Fluorescence Measurements of Coumarin 153. We recorded the absorption and emission spectra of C-153 in neat EAN and bmimPF$_6$. The absorption maximum of C-153 in neat EAN and bmimPF$_6$ was found to be 432 and 422 nm, respectively (Table 2). On the other hand, the emission maximum of C-153 in neat EAN and bmimPF$_6$ was found to be 550 and 530 nm, respectively. The emission spectra of C-153 in different systems are shown in Figure 7. With the addition of 0.37 M Triton X-100 in EAN, both the absorption and emission maxima blue-shifted to 425 and 537 nm, respectively. This 13 nm blue shift in emission maxima clearly indicates that the C-153 molecule locates itself inside the Triton X-100/EAN micellar aggregate where the polarity is less compared to that of neat EAN. In a similar way, with the addition of 0.82 M Triton X-100 in bmimPF$_6$, both the absorption and emission maxima blue-shifted to 417 and 517 nm, respectively. Once again, the 13 nm blue shift in emission maxima clearly indicates that the C-153 molecule resides inside the Triton X-100/bmimPF$_6$ micellar aggregate where the polarity is less compared to that of neat bmimPF$_6$. Further, with the gradual addition of EAN in solution containing Triton X-100/bmimPF$_6$ micellar aggregate, the absorption and emission maxima red-shifted to 420 and 521 nm, respectively. This red shift with the addition of EAN is another indication of EAN penetration inside Triton X-100/bmimPF$_6$ micellar aggregate, as suggested by methyl orange (MO) spectra and NMR studies.

Table 2. Steady State Absorption and Emission Maxima of C-153 in Different Systems

system	λ_{max}[a] (absorption, nm)	λ_{max}[a] (emission, nm)
bmimPF$_6$	422	530
bmimPF$_6$ + TX-100	417	517
bmimPF$_6$ + TX-100 + 0.6 wt % EAN	417	517
bmimPF$_6$ + TX-100 + 1.9 wt % EAN	418	518
bmimPF$_6$ + TX-100 + 4.3 wt % EAN	419	520
bmimPF$_6$ + TX-100 + 7.2 wt % EAN	419	521
bmimPF$_6$ + TX-100 + 11.0 wt % EAN	420	521
EAN	432	550
EAN + TX-100	425	537
EAN + TX-100 + 2.0 wt % bmimPF$_6$	425	536
EAN + TX-100 + 4.0 wt % bmimPF$_6$	424	536
EAN + TX-100 + 8.0 wt % bmimPF$_6$	424	535
EAN + TX-100 + 12.0 wt % bmimPF$_6$	423	535

[a]Error in experimental data of ±2 nm.

3.5. Time-Resolved Studies. *3.5.1. Solvation Dynamics.* We gathered information regarding the location of the probe molecule (C-153) inside the micellar aggregates by absorption and emission spectroscopy. In addition to this, the ^{1}H NMR and pulsed-field gradient spin−echo NMR (PFGSE NMR) measurements reveal information about the location of added RTILs in the micellar aggregates. To study the solvent relaxation dynamics (solvation dynamics), we have used C-153 as the probe molecule. To probe the change in the dynamics of solvent molecule around C-153 with the addition of Triton X-100 in neat ionic liquids and with the penetration of ionic liquids inside the micellar aggregates, we have collected the time-resolved decays monitored at different wavelengths for all the systems. In all the systems, the fluorescence decays of C-153 showed a huge dependence on the emission wavelength. At the red edge of emission spectra, the observed decay consists of a clear rise (growth) followed by usual decay, and at the blue end of emission spectra, a faster decay is observed which is a clear signature of the solvation dynamics. The representative decays of C-153 in Triton X-100/bmimPF$_6$ micellar aggregate containing 1.9 wt % EAN and Triton X-100/EAN micellar aggregate containing 2.0 wt % bmimPF$_6$ monitoring at different wavelengths at 298 K are shown in Figure S1 of the Supporting Information. The red edge and extreme blue edge decay profiles were best fitted by biexponential and triexponential functions, respectively. The time-resolved emission spectra (TRES) were constructed by the following procedure of Fleming and Maroncelli.[89,90] The TRES at a given time t, $S(\lambda; t)$, is obtained by the fitted decays, $D(t; \lambda)$, by relative normalization to the steady-state spectrum $S_0(\lambda)$, as follows

$$S(\lambda; t) = D(t; \lambda)\frac{S_0(\lambda)}{\int_0^\infty D(t; \lambda)\, dt} \quad (3)$$

Each time-resolved emission spectrum (TRES) was fitted by "log-normal line shape function", which is defined as

$$g(\nu) = g_0 \exp\left[-\ln 2\left(\frac{\ln[1 + 2b(\nu - \nu_p)/\Delta]}{b}\right)^2\right] \quad (4)$$

where g_0, b, ν_p, and Δ are the peak height, asymmetric parameter, peak frequency, and width parameter, respectively. The representative TRES plot of C-153 in Triton X-100/bmimPF$_6$ micellar aggregate containing 1.9 wt % EAN and Triton X-100/EAN micellar aggregate containing 2.0 wt % bmimPF$_6$ are shown in Figure S2 of the Supporting Information. The peak frequency evaluated from this log-normal fitting of TRES was then used to construct the decay of the solvent correlation function $C(t)$, which is defined as

$$C(t) = \frac{\nu(t) - \nu(\infty)}{\nu(0) - \nu(\infty)} \quad (5)$$

$\nu(0)$ is the frequency at "zero-time", as calculated by the full method of Fleming and Maroncelli.[89] $\nu(\infty)$ is the frequency at "infinite time", which may be taken as the maximum of the steady-state fluorescence spectrum if solvation is more rapid

dx.doi.org/10.1021/jp309106a | J. Phys. Chem. B 2012, 116, 13868−13877

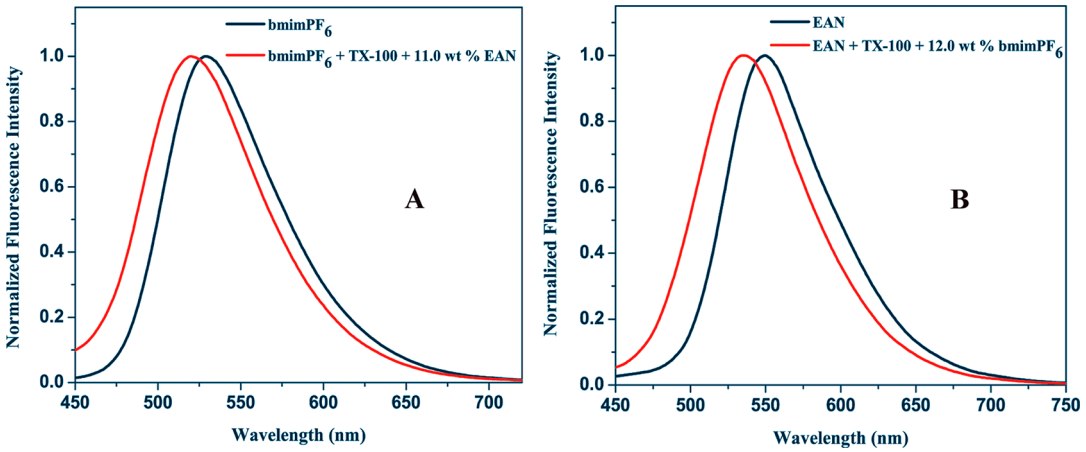

Figure 7. Emission spectra of C-153 in (A) neat bmimPF$_6$ and Triton X-100/bmimPF$_6$ micellar aggregate containing 11.0 wt % EAN and (B) neat EAN and Triton X-100/EAN micellar aggregate containing 12.0 wt % bmimPF$_6$.

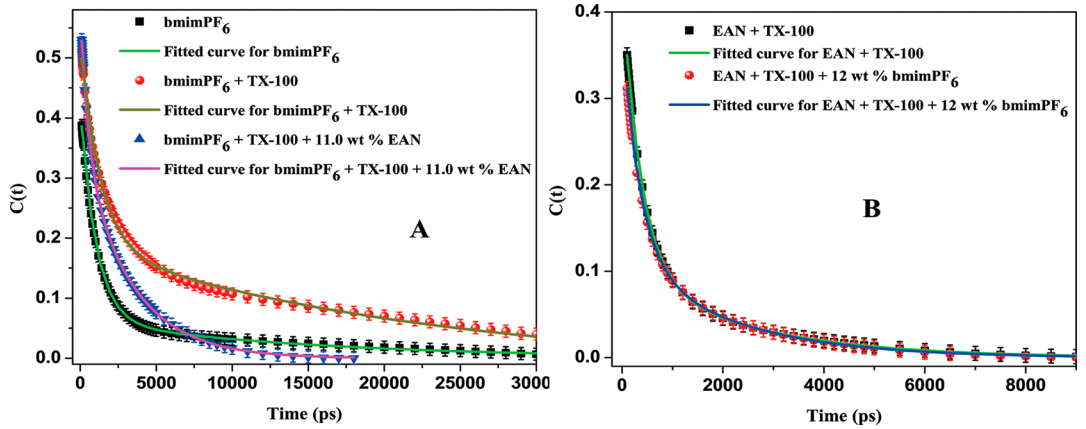

Figure 8. Decay of solvent correlation function $C(t)$ of C-153 in (A) neat bmimPF$_6$, Triton X-100/bmimPF$_6$ micellar aggregate, and the same micellar aggregate containing 11.0 wt % EAN and (B) Triton X-100/EAN micellar aggregate and same micellar aggregate containing 12.0 wt % bmimPF$_6$.

than the population decay of the probe. $\nu(t)$ is determined by taking the maxima from the log-normal fits as the emission maximum. In most of the cases, the spectra are broad, so there is some uncertainty in the exact position of the emission maxima. Therefore, following Petrich et al.,[91−93] we have considered the range of the raw data points in the neighborhood of the maximum to estimate an error for the maximum obtained from the log-normal fit. Depending on the width of the spectrum (i.e., zero-time, steady state, or TRES), we have determined the typical uncertainties as follows: zero time ≈ steady-state (110 cm^{-1}) < time-resolved (200 cm^{-1}) emission. We use these uncertainties to compute error bars for $C(t)$. Finally, in generating $C(t)$, the first point was obtained from the zero time spectrum. The second point was taken at the maximum of the instrument response function, which, having a full width at half-maximum of <100 ps, was taken to be 100 ps. Finally, the time dependence of the calculated $C(t)$ values was fitted by a biexponential function because χ^2 lies close to 1, which indicates the goodness of the fit. The biexponential function is as follows

$$C(t) = a_1 e^{-t/\tau_1} + a_2 e^{-t/\tau_2} \quad (6)$$

where τ_1 and τ_2 are the two solvation times (≥100 ps, below this we are missing owing to our instrumental resolution) with amplitudes of a_1 and a_2, respectively. The missing component can be defined as $(1 - (a_1 + a_2)) \times 100\%$. The $C(t)$ versus time plots are shown in Figure 8. The decay parameters of $C(t)$ are summarized in Table 3. The average solvation time is calculated as

$$\tau_{av} = a_1\tau_1 + a_2\tau_2 \quad (7)$$

The average solvation time of C-153 in neat bmimPF$_6$ was found to be 1.26 ns (Table 3) with components 1.04 ns (36.0%) and 14.77 ns (6.0%). The obtained average solvation time in neat bmimPF$_6$ differs from the average solvation time reported in our earlier manuscript.[94] This difference arises due to the difference in the construction of $C(t)$ (in our earlier manuscript, we have not excluded the missing component). The observed time constants change drastically with the addition of 0.82 M Triton X-100. The average solvation time of C-153 in Triton X-100/bmimPF$_6$ micellar aggregate was found to be 3.94 ns (Table 3) with components 1.24 ns (33.0%) and 17.65 ns (20.0%). Thus, the average solvation time increases by a factor of ∼3 on going from neat IL (bmimPF$_6$) to ionic liquid containing micellar aggregate. A similar type of behavior is observed in the case of EAN. Halder et al.[95] reported that the average solvation time of C-153 in neat EAN is 26 ps. We have used their data for the comparison with the Triton X-100/EAN micellar aggregate, because we are unable to detect the solvation dynamics for neat EAN with our instrumental

dx.doi.org/10.1021/jp309106a | J. Phys. Chem. B 2012, 116, 13868−13877

Table 3. Decay Parameters of $C(t)$ of C-153 in Different Systems

system	a_i (τ_i) (ns)	$\langle\tau_s\rangle^a$ (ns)	missing component (%)
$bmimPF_6$	0.36 (1.04), 0.06 (14.77)	1.26	58
$bmimPF_6$ + TX-100	0.33 (1.24), 0.20 (17.65)	3.94	47
$bmimPF_6$ + TX-100 + 0.6 wt % EAN	0.34 (1.23), 0.19 (14.95)	3.26	47
$bmimPF_6$ + TX-100 + 1.9 wt % EAN	0.35 (1.20), 0.20 (12.54)	2.93	45
$bmimPF_6$ + TX-100 + 7.2 wt % EAN	0.26 (0.81), 0.29 (5.16)	1.71	45
$bmimPF_6$ + TX-100 + 11.0 wt % EAN	0.22 (0.52), 0.35 (3.24)	1.25	43
EAN + TX-100	0.33 (0.36), 0.10 (2.38)	0.36	57
EAN + TX-100 + 2.0 wt % $bmimPF_6$	0.30 (0.30), 0.14 (1.94)	0.36	56
EAN + TX-100 + 4.0 wt % $bmimPF_6$	0.26 (0.33), 0.12 (2.05)	0.33	62
EAN + TX-100 + 8.0 wt % $bmimPF_6$	0.28 (0.34), 0.12 (1.93)	0.33	60
EAN + TX-100 + 12.0 wt % $bmimPF_6$	0.27 (0.34), 0.13 (2.05)	0.36	60

[a]Error in experimental data of ±100 ps.

setup. The average solvation time of C-153 in Triton X-100/EAN micellar aggregate was found to be 0.36 ns (Table 3) with components 0.36 ns (33.0%) and 2.38 ns (10.0%). Thus, here also the average solvation time increases by a factor of ∼14 on going from neat IL (EAN) to ionic liquid containing micellar aggregate. Not only this, similar behavior is observed in our earlier manuscript on going from neat IL to IL containing micellar aggregates.[96−99] Thus, we can conclude that the increase in solvation time on going from neat RTIL to RTIL containing micellar aggregate is very small compared to the increase in solvation time on going from pure water to water containing micelle (which is of the order of 100−1000 times). The huge retardation of solvation dynamics in the latter case arises due to extended hydrogen bonding between water and surfactant molecules, counterions, and the micellar head groups. Recent computer simulation[100] studies have shown that the hydrogen bonding between water molecules and surfactant is much stronger than the hydrogen bond between the two water molecules. On the other hand, unlike the 1000-fold retardation in solvation dynamics on going from water to water containing micelles, the little change in the solvation time on going from RTIL to RTIL containing micellar aggregates suggests (1) micellar aggregate formation has little effect on the interaction between the ions of RTIL and (2) the interaction between the surfactant and the RTIL is almost the same as the interaction between the ions of RTILs.

Further, with the gradual addition of EAN in solution containing Triton X-100/$bmimPF_6$ micellar aggregate, the average solvation time of C-153 decreases (Figure 8A). On going from Triton X-100/$bmimPF_6$ micellar aggregate to micellar aggregate containing 11.0 wt % EAN, the average solvation time changes from 3.94 to 1.25 ns (Table 3). This decrease in average solvation time once again indicates EAN penetration inside Triton X-100/$bmimPF_6$ micellar aggregate, as indicated by red shift in absorption maxima of methyl orange (MO), NMR studies, and red shift in absorption and emission maxima of C-153. Contrary to this, the average solvation time of C-153 remains the same with the addition of $bmimPF_6$ in Triton X-100/EAN micellar aggregate (Figure 8B). On going from Triton X-100/EAN micellar aggregate to micellar aggregate containing 12.0 wt % $bmimPF_6$, the average solvation time remains unchanged (0.36 ns). This clearly indicates that the penetration of $bmimPF_6$ in Triton X-100/EAN micellar aggregates does not affect the local environment of C-153.

4. CONCLUSION

In conclusion, we have successfully characterized micellar aggregates of Triton X-100 with a mixture of two RTILs, $bmimPF_6$ and EAN. The EAN molecule penetrates to the Triton X-100/$bmimPF_6$ micellar aggregate, which is well supported by (i) the red shift in absorption maxima of methyl orange (MO), (ii) ^1H NMR, and (iii) the red shift in absorption and emission maxima of C-153. On the other hand, with the addition of $bmimPF_6$ to Triton X-100/EAN micellar aggregate, the absorption spectra of MO and emission spectra of C-153 remain unaffected. This indicates that the micro-environment around the probe molecules remains unaffected. The average solvation time of C-153 decreases with the addition of EAN in Triton X-100/$bmimPF_6$ micellar aggregates, whereas it remains constant with the addition of $bmimPF_6$ in Triton X-100/EAN micellar aggregate. This further supports the conclusions drawn from UV−visible and NMR studies. It is also noteworthy to mention that the solvent relaxation around C-153 gets retarded on going from neat ILs to the micellar solution of Triton X-100 in ILs. The extent of retardation (∼10 times) clearly indicates that the micellar aggregate formation has little effect on the interaction between the ions of RTILs. This leads to a small increase in average solvation time compared to the increase observed on going from pure water to water containing micellar aggregates (100−1000 times). Thus, we have certainly established a class of hybrid environmentally benign systems composed of all nonvolatile components. These systems have potential for application at high temperature in different fields of interest.[51]

■ ASSOCIATED CONTENT

Supporting Information

The fluorescence decays and TRES plots. This material is available free of charge via the Internet at http://pubs.acs.org.

■ AUTHOR INFORMATION

Corresponding Author

*Fax: 91-3222-255303. Phone: 91-3222-283332. E-mail: nilmoni@chem.iitkgp.ernet.in.

Notes

The authors declare no competing financial interest.

■ ACKNOWLEDGMENTS

N.S. thanks the Council of Scientific and Industrial Research (CSIR) and Government of India for generous research grants. V.G.R., S.M., and S.G. are thankful to CSIR, and C.B. is thankful to UGC for a research fellowship. The authors are thankful to DST FIST for funding the NMR equipment.

■ REFERENCES

(1) Jaramillo, T. F.; Baeck, S. H.; Cuenya, B. R.; McFarland, E. W. *J. Am. Chem. Soc.* **2003**, *125*, 7148−7149.

(2) Savic, R.; Luo, L. B.; Eisenberg, A.; Maysinger, D. *Science* **2003**, *300*, 615−618.

(3) Alexandridis, P., Lindman, B., Eds.; *Amphiphilic Block Copolymers: Self-Assembly and Applications*; Elsevier: Amsterdam, The Netherlands, 2000.
(4) He, Y. Y.; Li, Z. B.; Simone, P.; Lodge, T. P. *J. Am. Chem. Soc.* **2001**, *128*, 2745−2750.
(5) Evans, D. F. *Langmuir* **1988**, *4*, 3−12.
(6) Ward, A. J. I.; Du Reau, C. Surfactant Association in Nonaqueous Media. In *Surface and Colloid Science*; Matijevic, E., Ed.; Plenum Press: New York, 1993; Vol. *15*, Chapter 4.
(7) Eastoe, J.; Gold, S.; Rogers, S.; Wyatt, P.; Steytler, D. C.; Gurgel, A.; Heenan, R. K.; Fan, X.; Beckman, E. J.; Enick, R. M. *Angew. Chem., Int. Ed.* **2006**, *45*, 3675−3677.
(8) Sagisaka, M.; Iwama, S.; Yoshizawa, A.; Mohamed, A.; Cummings, S.; Eastoe, J. *Langmuir* **2012**, *28*, 10988−10996.
(9) Mohamed, A.; Sagisaka, M.; Hollamby, M.; Rogers, S. E.; Heenan, R. K.; Dyer, R.; Eastoe, J. *Langmuir* **2012**, *28*, 6299−6306.
(10) Seddon, K. R. *Nature* **2003**, *2*, 363−364.
(11) Welton, T. *Chem. Rev.* **1999**, *99*, 2071−2084.
(12) Plechkova, N. V.; Seddon, K. R. *Chem. Soc. Rev.* **2008**, *37*, 123−150.
(13) Ranke, J.; Stolte, S.; Stormann, R.; Arning, J.; Jastorff, B. *Chem. Rev.* **2007**, *107*, 2183−2206.
(14) Rodgers, R. D.; Seddon, K. R. *Science* **2003**, *302*, 792−793.
(15) Forsyth, S. A.; Pringle, J. M.; MacFarlane, D. R. *Aust. J. Chem.* **2004**, *57*, 113−119.
(16) Evans, D. F.; Yamauchl, A.; Roman, R.; Casassa, E. Z. *J. Colloid Interface Sci.* **1982**, *88*, 89−96.
(17) Evans, D. F.; Yamauchl, A.; Jason Wel, G.; Bloomfield, V. A. *J. Phys. Chem.* **1983**, *87*, 3537−3541.
(18) Anderson, J. L.; Pino, V.; Hagberg, E. C.; Sheares, V. V.; Armstrong, D. W. *Chem. Commun.* **2003**, 2444−2445.
(19) Patrascu, C.; Gauffre, F.; Nallet, F.; Bordes, R.; Oberdisse, J.; de Lauth-Viguerie, N. *ChemPhysChem* **2006**, *7*, 99−101.
(20) Tang, J.; Li, D.; Sun, C. Y.; Zheng, L. Z.; Li, J. H. *Colloids Surf., A* **2006**, *273*, 24−28.
(21) Velasco, S. B.; Turmine, M.; Di Caprio, D.; Letellier, P. *Colloids Surf., A* **2006**, *275*, 50−54.
(22) Thomaier, S.; Kunz, W. *J. Mol. Liq.* **2007**, *130*, 104−107.
(23) Fletcher, K. A.; Pandey, S. *Langmuir* **2004**, *20*, 33−36.
(24) Behera, K.; Dahiya, P.; Pandey, S. *J. Colloid Interface Sci.* **2007**, *307*, 235−245.
(25) He, Y. Y.; Lodge, T. P. *J. Am. Chem. Soc.* **2006**, *128*, 12666−12667.
(26) Greaves, T. L.; Drummond, C. J. *Chem. Rev.* **2008**, *108*, 206−237.
(27) Gao, H. X.; Li, J. C.; Han, B. X.; Chen, W. N.; Zhang, J. L.; Zhang, R.; Yan, D. D. *Phys. Chem. Chem. Phys.* **2004**, *6*, 2914−2916.
(28) Eastoe, J.; Gold, S.; Rogers, S. E.; Paul, A.; Welton, T.; Heenan, R. K.; Grillo, I. *J. Am. Chem. Soc.* **2005**, *127*, 7302−7303.
(29) Greaves, T. L.; Weerawardena, A.; Krodkjewska, I.; Drummond, C. J. *J. Phys. Chem. B* **2008**, *112*, 896−905.
(30) Gao, Y. A.; Li, N.; Zheng, L. Q.; Bai, X. T.; Yu, L.; Zhao, X. Y. *J. Phys. Chem. B* **2007**, *111*, 2506−2513.
(31) Li, N.; Gao, Y. A.; Zheng, L. Q.; Zhang, J.; Yu, L.; Li, X. W. *Langmuir* **2007**, *23*, 1091−1097.
(32) Atkin, R.; Warr, G. G. *J. Phys. Chem. B* **2007**, *111*, 9309−9316.
(33) Gao, Y. A.; Li, N.; Zheng, L. Q.; Zhao, X. Y.; Zhang, J.; Cao, Q. *Chem.—Eur. J.* **2007**, *13*, 2661−2670.
(34) Zech, O.; Thomaier, S.; Kolodziejski, A.; Touraud, D.; Grillo, I.; Kunz, W. *Chem.—Eur. J.* **2010**, *16*, 783−786.
(35) Zech, O.; Thomaier, S.; Bauduin, P.; Rück, T.; Touraud, D.; Kunz, W. *J. Phys. Chem. B* **2009**, *113*, 465−473.
(36) Gayet, F.; El Kalamouni, C.; Lavedan, P.; Marty, J. D.; Brûlet, A.; Lauth-de Viguerie, N. *Langmuir* **2009**, *25*, 9741−9750.
(37) Zhou, Y; Qiu, L.; Deng, Z.; Texter, J.; Yan, F. *Macromolecules* **2011**, *44*, 7948−7955.
(38) Adhikari, A.; Sahu, K.; Dey, S.; Ghosh, S.; Mandal, U.; Bhattacharyya, K. *J. Phys. Chem. B* **2007**, *111*, 12809−12816.
(39) Gao, Y. A.; Han, S. B.; Han, B. X.; Li, G. Z.; Shen, D.; Li, Z. H. *Langmuir* **2005**, *21*, 5681−5684.
(40) Cheng, S. Q.; Zhang, J. L.; Zhang, Z. F.; Han, B. X. *Chem. Commun.* **2007**, 2497−2499.
(41) Liu, J. H.; Cheng, S. Q.; Zhang, J. L.; Feng, X. Y.; Fu, X. G.; Han, B. X. *Angew. Chem., Int. Ed.* **2007**, *46*, 3313−3315.
(42) Seth, D.; Chakraborty, A.; Setua, P.; Sarkar, N. *Langmuir* **2006**, *22*, 7768−7775.
(43) Hao, J. C.; Song, A. X.; Wang, J. Z.; Chen, X.; Zhuang, W. C.; Shi, F. *Chem.—Eur. J.* **2005**, *11*, 3936−3940.
(44) He, Y. Y.; Boswell, P. G.; Buhlmann, P.; Lodge, T. P. *J. Phys. Chem. B* **2007**, *111*, 4645−4652.
(45) Evans, D. F.; Kaler, E. W.; Benton, W. J. *J. Phys. Chem.* **1983**, *87*, 533−535.
(46) Araos, M. U.; Warr, G. G. *J. Phys. Chem. B* **2005**, *109*, 14275−14277.
(47) Wu, J.; Li, N.; Zheng, L.; Li, X.; Gao, Y.; Inoue, T. *Langmuir* **2008**, *24*, 9314−9322.
(48) Li, N.; Zhang, S.; Zheng, L.; Inoue, T. *Langmuir* **2009**, *25*, 10473−10482.
(49) Inoue, T. *J. Colloid Interface Sci.* **2009**, *337*, 240−246.
(50) Gao, Y.; Li, N.; Li, X.; Zhang, S.; Zheng, L.; Bai, X.; Yu, L. *J. Phys. Chem. B* **2009**, *113*, 123−130.
(51) Zhao, Y.; Chen, X.; Wang, X. *J. Phys. Chem. B* **2009**, *113*, 2024−2030.
(52) Shim, Y.; Jeong, D.; Manjari, S.; Choi, M. D.; Kim, H. J. *Acc. Chem. Res.* **2007**, *40*, 1130−1137.
(53) Paul, A.; Samanta, A. *J. Phys. Chem. B* **2007**, *111*, 4724−4731.
(54) Arzhantsev, S.; Jin, H.; Baker, G. A.; Maroncelli, M. *J. Phys. Chem. B* **2007**, *111*, 4978−4989.
(55) Baker, S. N.; Baker, G. A.; Munson, C. A.; Chen, F.; Bukowski, E. J.; Cartwright, A. N.; Bright, F. V. *Ind. Eng. Chem. Res.* **2003**, *42*, 6457−6463.
(56) Hu, Z.; Margulis, C. J. *Acc. Chem. Res.* **2007**, *40*, 1097−1105.
(57) Adhikari, A.; Dey, S.; Das, D. K.; Mandal, U.; Ghosh, S.; Bhattacharyya, K. *J. Phys. Chem. B* **2008**, *112*, 6350−6357.
(58) Hu, Z.; Margulis, C. J. *J. Phys. Chem. B* **2006**, *110*, 11025−11028.
(59) Aki, S. N. V. K.; Brennecke, J. F.; Samanta, A. *Chem. Commun.* **2001**, 413−414.
(60) Paul, A.; Mandal, P. K.; Samanta, A. *J. Phys. Chem. B* **2005**, *109*, 9148−9153.
(61) Ito, N.; Arzhantsev, S.; Maroncelli, M. *Chem. Phys. Lett.* **2004**, *396*, 83−91.
(62) Chakrabarty, D.; Hazra, P.; Chakraborty, A.; Seth, D.; Sarkar, N. *Chem. Phys. Lett.* **2003**, *381*, 697−704.
(63) Karmakar, R.; Samanta, A. *J. Phys. Chem. A* **2002**, *106*, 6670−6675.
(64) Nandi, N.; Bhattacharyya, K.; Bagchi, B. *Chem. Rev.* **2000**, *100*, 2013−2046.
(65) Bagchi, B. *Chem. Rev.* **2005**, *105*, 3197−3219.
(66) Bagchi, B.; Jana, B. *Chem. Soc. Rev.* **2010**, *39*, 1936−1954.
(67) Kumbhakar, M.; Nath, S.; Mukherjee, T.; Pal, H. *J. Chem. Phys.* **2004**, *121*, 6026−6033.
(68) Willard, D. M.; Riter, R. E.; Levinger, N. E. *J. Am. Chem. Soc.* **1998**, *120*, 4151−4160.
(69) Pal, S. K.; Zewail, A. H. *Chem. Rev.* **2004**, *104*, 2099−2124.
(70) Pal, S. K.; Zhao, L.; Zewail, A. H. *Proc. Natl Acad. Sci. U.S.A.* **2003**, *100*, 8113−8118.
(71) Zhong, D.; Pal, S. K.; Zewail, A. H. *Chem. Phys. Lett.* **2011**, *503*, 1−11.
(72) Bhattacharyya, K. *Chem. Commun.* **2008**, 2848−2857.
(73) Bhattacharyya, K. *Acc. Chem. Res.* **2003**, *36*, 95−101.
(74) Castner, E. W., Jr.; Wishart, J. F.; Shirota, H. *Acc. Chem. Res.* **2007**, *40*, 1217−1227.
(75) Shirota, H.; Funston, A. M.; Wishart, J. F.; Castner, E. W., Jr. *J. Chem. Phys.* **2005**, *122*, 184512−184523.
(76) Jin, H.; Baker, G. A.; Arzhantsev, S.; Dong, J.; Maroncelli, M. *J. Phys. Chem. B* **2007**, *111*, 7291−7302.

(77) Funston, A. M.; Fadeeva, T. A.; Wishart, J. F.; Castner, E. W., Jr. *J. Phys. Chem. B* **2007**, *111*, 4963−4977.
(78) Kobrak, M. N. *J. Chem. Phys.* **2006**, *125*, 064502−064513.
(79) Jeong, D.; Shim, Y.; Choi, M. Y.; Kim, H. J. *J. Phys. Chem. B* **2007**, *111*, 4920−4925.
(80) Kashyap, H. K.; Biswas, R. *J. Phys. Chem. B* **2008**, *112*, 12431−12438.
(81) Kashyap, H. K.; Biswas, R. *J. Phys. Chem. B* **2010**, *114*, 254−268.
(82) Mukherjee, P.; Crank, J. A.; Halder, M.; Armstrong, D. W.; Petrich, J. W. *J. Phys. Chem. A* **2006**, *110*, 10725−10730.
(83) Das, K. P.; Ceglie, A.; Lindman, B. *J. Phys. Chem.* **1987**, *91*, 2938−2946.
(84) Kumbhakar, M.; Goel, T.; Mukherjee, T.; Pal, H. *J. Phys. Chem. B* **2004**, *108*, 19246−19254.
(85) Hazra, P.; Chakrabarty, D.; Sarkar, N. *Langmuir* **2002**, *18*, 7872−7879.
(86) Zhu, D. M.; Schelly, Z. A. *Langmuir* **1992**, *8*, 48−50.
(87) Li, N.; Zhang, S.; Ma, H.; Zheng, L. *Langmuir* **2010**, *26*, 9315−9320.
(88) Tanner, J. E.; Stejskal, E. O. *J. Chem. Phys.* **1968**, *49*, 1768−1777.
(89) Fee, R. S.; Maroncelli, M. *Chem. Phys.* **1994**, *183*, 235−247.
(90) Maroncelli, M.; Fleming, G. R. *J. Chem. Phys.* **1987**, *86*, 6221−6239.
(91) Bose, S.; Adhikary, R.; Mukherjee, P.; Song, X.; Petrich, J. W. *J. Phys. Chem. B* **2009**, *113*, 11061−11068.
(92) Headley, L. S.; Mukherjee, P.; Anderson, J. L.; Ding, R.; Halder, M.; Armstrong, D. W.; Song, X.; Petrich, J. W. *J. Phys. Chem. A* **2006**, *110*, 9549−9554.
(93) Mukherjee, P.; Crank, J. A.; Sharma, P. S.; Wijeratne, A. B.; Adhikary, R.; Bose, S.; Armstrong, D. W.; Petrich, J. W. *J. Phys. Chem. B* **2008**, *112*, 3390−3396.
(94) Chakraborty, A.; Seth, D.; Chakrabarty, D.; Setua, P.; Sarkar, N. *J. Phys. Chem. A* **2005**, *109*, 11110−11116.
(95) Halder, M.; Headley, L. S.; Mukherjee, P.; Song, X.; Petrich, J. W. *J. Phys. Chem. A* **2006**, *110*, 8623−8626.
(96) Rao, V. G.; Ghatak, C.; Pramanik, R.; Sarkar, S.; Sarkar, N. *Chem. Phys. Lett.* **2010**, *499*, 89−93.
(97) Rao, V. G.; Ghatak, C.; Pramanik, R.; Sarkar, S.; Sarkar, N. *J. Phys. Chem. B* **2011**, *115*, 10500−10508.
(98) Seth, D.; Chakraborty, A.; Setua, P.; Sarkar, N. *J. Phys. Chem. B* **2007**, *111*, 4781−4787.
(99) Rao, V. G.; Mandal, S.; Ghosh, S.; Banerjee, C.; Sarkar, N. *J. Phys. Chem. B* **2012**, *116*, 8210−8221.
(100) Balasubramanian, S.; Pal, S.; Bagchi, B. *Phys. Rev. Lett.* **2002**, *89*, 115505−115508.